# Supporting Information

Experimental and theoretical study on the transformation behavior of bisphenol S by radicals driven persulfate oxidation

Junyan Wei[1], Linning Yin[1], Ruijuan Qu[1], Gadah Al-Basher[2], Xiaoxue Pan[1, 3*], Zunyao Wang[1*]

[1] *State Key Laboratory of Pollution Control and Resources Reuse, School of the Environment, Nanjing University, Nanjing 210023, Jiangsu, PR China*

[2] *King Saud University, College of Science, Zoology Department, P.O. Box 2455, Riyadh, 11451, Saudi Arabia*

[3] *School of Resources and Environmental Engineering, Anhui University, Anhui Hefei 230601, PR China*

[*]Corresponding author: Xiaoxue Pan and Zunyao Wang.

E-mail address: panxiaoxue1208@163.com and wangzy@nju.edu.cn.

Tel: +86-0551-63861985 and +86-25-89680358;

Fax: +86-0551-63861985 and +86-25-89680358.

**Pages: 37.**

**Text: 5.**

**Figures: 14.**

**Tables: 8.**

**Text. S1.** Reagents and water matrices

BPS ($C_{12}H_{10}O_4S$, purity ≥ 99%) was obtained from Aladdin (Shanghai, China). Multi-walled carbon nanotubes (MWCNTs), single-walled carbon nanotubes (SWCNTs), hydroxylated multi-walled carbon nanotubes (CNT-OH), graphene (GP) and graphite oxide (GO) were purchased from Shenzhen Nanotech Port Co., Ltd (Shenzhen, China), and their properties were summarized in Tables S1, S2 and S3. Methanol, *tert*-butanol and 5,5-dimethyl-pyrroline-*N*-oxide (DMPO) were obtained from J&K Scientific Ltd. (Beijing, China). Potassium persulfate ($K_2S_2O_8$, purity ≥ 99.5%), and other reagents (analytical grade at least) were purchased from Nanjing Chemical Reagent Co., Ltd (Nanjing, China) without further purification.

Secondary effluent and River water were collected from the Wulongkou sewage treatment plant (Zhengzhou, China) and Jiuxiang River (Nanjing, China), respectively, and they were filtered through 0.45 μm glass fiber membranes (GF/F, Waterman, Maidstone, UK) before use. Tap water was sampled from our lab (Nanjing, China). Main physicochemical parameters of the four water samples were listed in Table S4. Unless otherwise stated, ultrapure water (18.25 MΩ cm), produced with a Milli-Q water purification system, was used in all experiments.

**Text. S2.** Preparation and characterization of nitrogen-doped nanocarbon based materials

Our previous work has proved that ammonium nitrate ($NH_4NO_3$) is the best nitrogen source among $NH_4NO_3$, urea, polyaniline and indole when we explored the effects of N from different reagents doping on hydroxylated multi-walled carbon nanotubes to catalyze PS for UV-type filter elimination.[1] Therefore, in this study, $NH_4NO_3$ was also used in order to further improve the removal efficiency of BPS. First, it was ground with carbonaceous materials at a mass ratio of 1:2 in an agate mortar. The above mixture was then placed into a tube furnace and kept at 350 ℃ for 1 h under continuous nitrogen gas flow. After calcined, the materials were reground and washed. Different $NH_4NO_3$-doped carbonaceous materials were abbreviated as N-MWCNTs, N-SWCNTs, N-CNT-OH, N-GO and N-GP.

Characterization of the prepared nanocarbon-based materials including scanning electron microscopy (SEM), transmission electron microscopy (TEM), X-ray photoelectron spectroscopy (XPS), Fourier transform infrared spectrometer (FT-IR), and BET surface area were performed and the used equipments in detail were recorded elsewhere.[1]

Fig. S1 showed the SEM and TEM images of SWCNTs (a and c) and N-SWCNTs (b and d), which confirmed that the tubular structure of SWCNT still remained after nitrogen doping. In addition, N-SWCNTs were more easily dispersed than SWCNTs, revealing that nitrogen doping might improve the dispersion of CNTs, which further resulted in the increased specific surface area (560.44 and 619.59 $m^2 \cdot g^{-1}$ of SWCNTs and N-SWCNTs respectively, listed in Table. S3). This phenomenon was also obtained in other materials except for GP (Table. S3), confirming nitrogen doping can enlarge the specific area of nanocarbon-based materials.

From XPS spectra (Fig. S2), the specific elemental composition of SWCNTs (a) and N-SWCNTs

(b) was summarized in Table. S2. Clearly, N did appear in N-SWCNTs samples, suggesting the successful doping of N into SWCNTs. Although the same synthesis method used in this and previous work,[1] more N content on the surface of N-SWCNTs was observed (1.16% versus 0.88%), which might be due to the existence of oxygen-containing functional groups on the surface of CNT-OH.[2]

As seen from the FT-IR spectra (Fig. S4), there are three obvious absorption peaks for both SWCNTs and N-SWCNTs. The bands around 3415 and 1100 $cm^{-1}$ were ascribed to the existence of hydroxyl groups (-OH), while the peak near 1560 $cm^{-1}$ could be attributed to the C=O stretching vibration of the carboxylic group (-COOH).[3] Compared to SWCNTs, the intensities of these three peaks were significantly increased in N-SWCNTs, meaning that the contents of surface oxygenic functional groups on SWCNTs were improved in the process of material preparation.

**Text. S3** Analytic method of intermediates

The mobile phase was consisted of 0.1% formic acid in water (A) and methanol (B), and the flow rate was 300 μL $min^{-1}$. The gradient elution program for LC-MS detection was given as 10% B (0 ~ 4.5 min), 40% B (4.5 ~ 7.5 min), 50% B (7.5 ~ 9 min), 80% B (9 ~ 11.5 min), 90% B (11.5 ~ 15 min), 95% B (15 ~ 18 min), 100% B (18 ~ 25.5 min), and 10% B (25.5 ~ 30 min). While 100% methanol was used for LC-MS/MS analysis at 300 μL $min^{-1}$ and current running time was just 5 min in total. The calibration error was kept below 3 ppm by using an electron spray ionization negative calibration solution (AB Sciex Pte. Ltd., USA). The operating parameters of the TOF 65 detector were set as follows: ion spray voltage floating, -4500 V (negative mode); temperature, 550 °C; ion source gas 1, 55 psi; ion source gas 2, 55 psi; curtain gas, 35 psi; declustering potential, -80 V; collision energy, -10 V; and scan range (m/z), 60 – 1500 amu. MS/MS analysis was performed using the same parameters except that the fragmentation was optimized by varying collision energy from 20 to 65 eV. All data were analyzed by using the SCIEX OS 1.6 software (AB Sciex).

**Text. S4** The efficiency of different nanocarbon-based materials

Under the conditions of 1.0 mM PS, 25 ℃, 30 $mg \cdot L^{-1}$ catalyst and initial pH 7.0, the adsorption and degradation kinetics of 10 μM BPS were carried out in nanocarbon-based catalyst/PS system. As shown in Fig. S5, all the materials could reach adsorption-desorption equilibrium after 30 min shaking. 24.0%, 63.3%, 14.6%, 1.0% and 9.8% of 10 μM BPS were adsorbed by MWCNTs, SWCNTs, CNT-OH, GO and GP, respectively, while a bit increase was achieved after N doping except for CNT-OH (their saturated adsorption capacities were similar). The adsorption content of each catalyst was highly surface area-dependent and thus large surface area (560.44 $m^2 \cdot g^{-1}$, listed in Table. S3) led to the highest adsorption for SWCNTs case. After adding PS, BPS was gradually degraded. Compared to PS alone, in which only 4.8% BPS removal was obtained, the removal efficiency of BPS in nanocarbon-based materials/PS systems ranged from 16.7% to 100.0% not including GO. The above results demonstrated that the presence of carbonaceous materials significantly improved the removal efficiency of BPS; and both the adsorption and the oxidative degradation contributed to the removal of BPS, which were further enhanced after N doping (Figs.1 (d) and S5), in good agreement with other findings.[4-6] This promoted effect could be attributed to the facts that N doping interrupts graphitic carbon configuration and then generates more active sites, changes electron states of the carbon network[7] and enhances the π–π bond of the carbon matrix.[4] The highest removal of BPS was observed in MWCNTs and SWCNTs situations (84.7%~100.0%) whether N doping or not, in comparison with CNT-OH, GP, and GO (2.0%~21.7%). This might be explained by the fact that the bent graphene sheets of CNTs included partially delocalized π electrons; these π electrons could provide better access to PS for target compounds.[8] Due to their highly $sp^2$-hybridized graphitic carbon skeletons with few defects and low

oxygen content, Duan *et al.* further verified the significant role of free-flowing π electrons in motivating PS.[9] However, Wang *et al.* found that nitrogen modification of reduced GO presented good activated PS performance to remove BPA;[10] Pan *et al.* reported the excellent catalytic ability of CNT-OH instead of CNT in 2,4,4'-trihydroxybenzophenone/PS solution.[1] The combined observation possibly suggested the selective catalytic performance of nanocarbon-based materials towards PS. In addition, the characters of target organic compounds should be taken into consideration, too.

**Text. S5** Catalytic mechanism

Accroding to recent reaserches, radical and non-radical mechanisms, including sulfate radicals ($SO_4^{\bullet-}$),[10] hydroxyl radicals (•OH),[11] singlet oxygen generation ($^1O_2$),[12, 13] PS-catalyst complex and electron transfer,[14, 15] are proved to exist in PS activation driven by nanocarbon-based materials. To explore the possible reactive species in PS/N-SWCNTs system, EPR and radical quenching experiments were conducted and the results were shown in Fig. S9. From EPR spectra (Fig. S9 (a)), it was seen that obvious peak of DMPO-OH adduct (hyperfine splitting constants of $\alpha_N = \alpha_H = 14.9$ G) was observed in PS+DMPO system, in comparison to single DMPO and N-SWCNTs. After adding N-SWCNTs, this signal intensity was largely improved. It was unexpected that no peak of DMPO-$SO_4$ adduct was recorded in all studied systems, which was contradictory with the identified sulfate addition intermediates (P5). A small amount of $SO_4^{\bullet-}$, fast transformation of DMPO-$SO_4$ adduct to DMPO-OH adduct and very strong intensity of DMPO-OH adduct might together lead to the disappearance of sulfate radicals signal.[16]

The radical quenching experiments were conducted to further validate the above observations of EPR spectra. Common $SO_4^{\bullet-}$ and •OH scavengers namely methanol and *tert*-tutanol were used. Herein, *tert*-tutanol can quench •OH at a rate constant of (3.8-7.6) $\times 10^8$ $M^{-1}$ $s^{-1}$, while methanol can quench both $SO_4^{\bullet-}$ and •OH and the corresponding rate constants were $2.5\times10^7$ and $9.7\times10^8$ $M^{-1}$ $s^{-1}$. As shown in Fig. S9 (b), compared to control, the residual of BPS in reaction solution after adding 100 mM *tert*-butanol increased from 6.1% to 26.2% in 60 min, and more BPS (72.2%) remained in solution at higher *tert*-butanol dosage. In contrary to *tert*-butanol, the addition of methanol did not show any inhibitory effect on BPS degradation even though its molar concentration was 50000 times as high as BPS. Similar findings were also obtained in previous studies.[17] This quenching inability

of methanol might be related with its more hydrophilic property than *tert*-butanol, which resulted in hard approach to the catalyst surface, and further failed quenching radicals on the surface of catalyst. From combined analysis of EPR results and quenching tests, we concluded that surface •OH radical ($•OH_{ads}$) was the primary ROS contributing to BPS removal.Other ROS like $SO_4^{•-}$ and $^1O_2$ might be also involved in the oxidative reaction, which was reflected by the incomplete quenching phenomenon of *tert*-butanol. Duan *et al.* also diclosed that N-SWCNTs could effectively activate PS to generate large amounts of •OH along with a small number of $SO_4^{•-}$.[11]

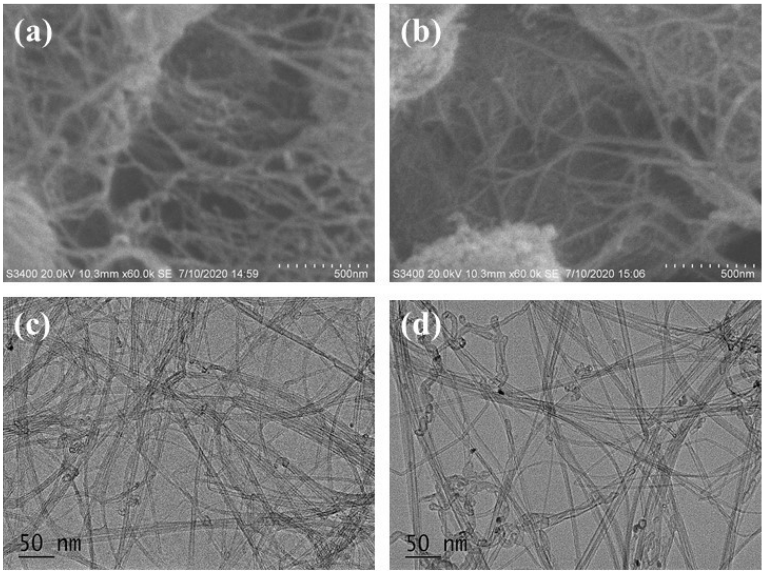


**Fig. S1.** SEM and TEM images of SWCNTs (a and c), N-SWCNTs (b and d).

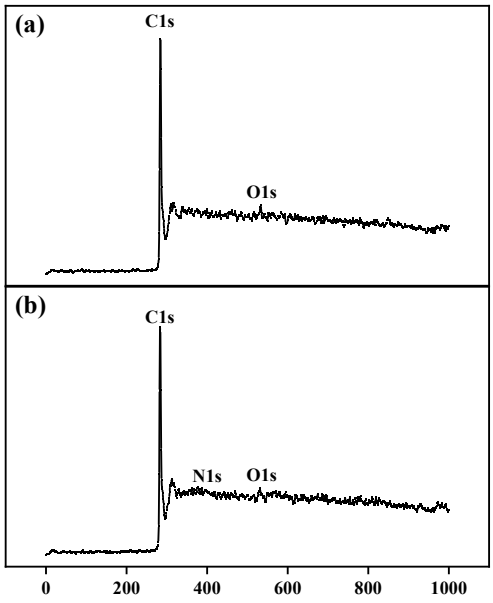


**Fig. S2.** XPS survey spectra of SWCNTs (a) and N-SWCNTs (b).

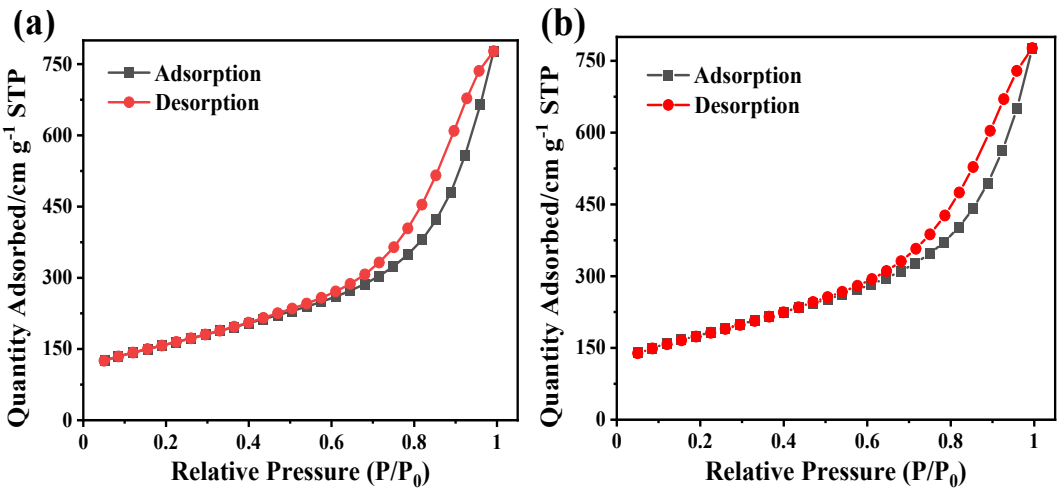


**Fig. S3.** $N_2$ adsorption-desorption isotherm of SWCNTs (a) and N-SWCNTs (b).

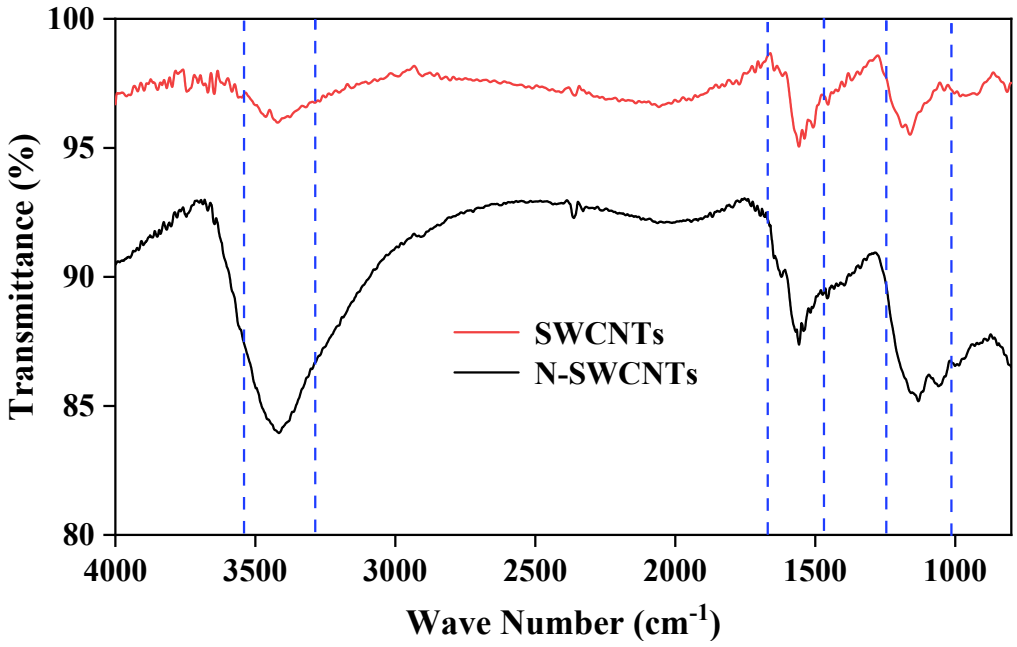


**Fig. S4.** FT-IR spectra of SWCNTs and N-SWCNTs.

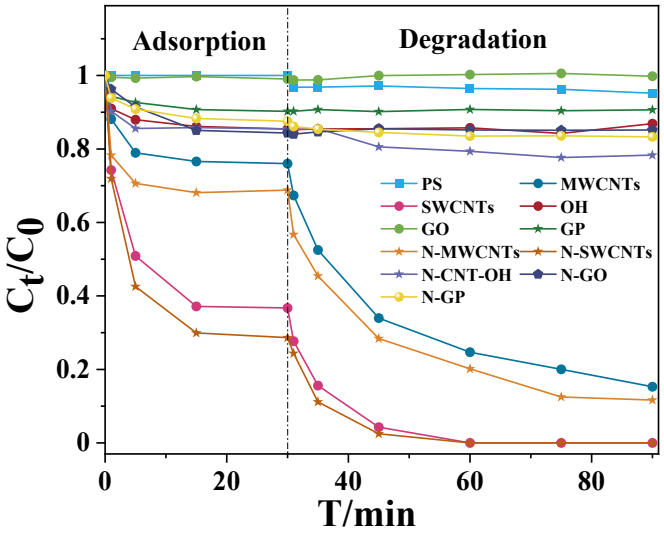


**Fig. S5.** Removal of BPS by five nanocarbon-based materials and their corresponding catalysts after N doping catalyzed PS. Conditions: $[BPS]_0$ = 10 μM, $[PS]_0$ = 1.0 mM, T = 25 ℃, $pH_0$ = 7.0, concentration of carbonaceous materials = 30 mg·$L^{-1}$.

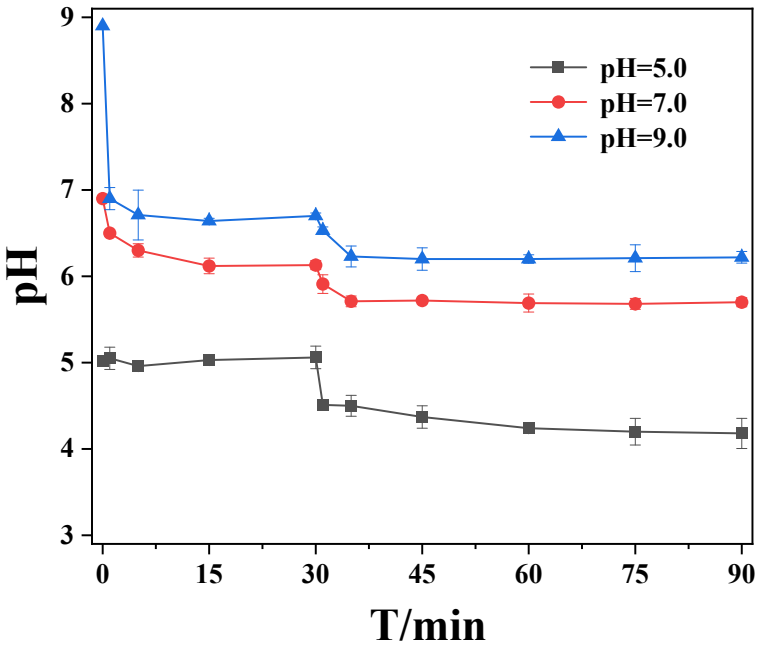


**Fig. S6**. The change of pH value during the reaction at different initial pH. Conditions: $[BPS]_0$ = 10 μM, $[PS]_0$ = 1.0 mM, T = 25 ℃, concentration of N-SWCNTs = 20 mg L.

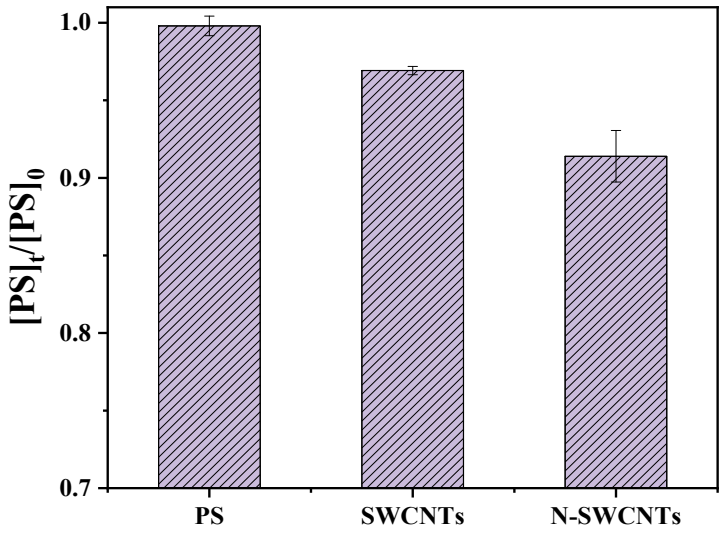


**Fig. S7.** Residual concentration of PS in three different systems. Conditions: $[BPS]_0$ = 10 μM, $[PS]_0$ = 1.0 mM, T = 25 ℃, $pH_0$ = 7.0, concentration of SWCNTs or N-SWCNTs = 20 $mg \cdot L^{-1}$.

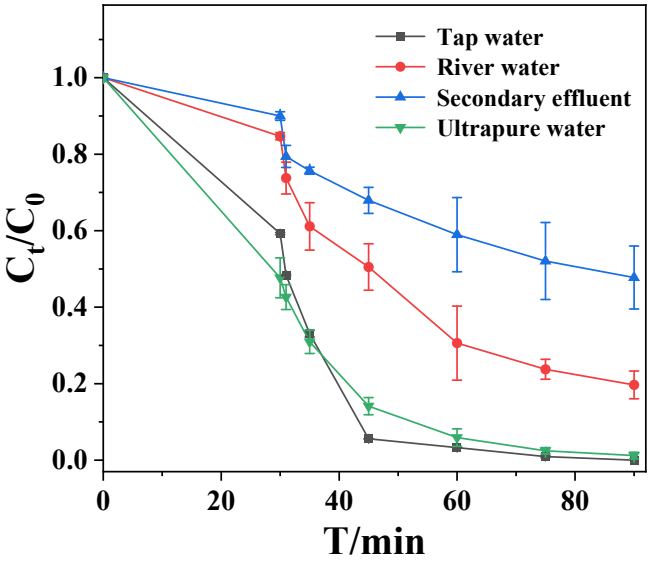


**Fig. S8.** Effect of water matrix on the degradation of BPS in PS/N-SWCNTs system. Conditions:

$[BPS]_0$ = 10 μM, $[PS]_0$ = 1.0 mM, T = 25 ℃, concentration of N-SWCNTs = 20 $mg \cdot L^{-1}$.

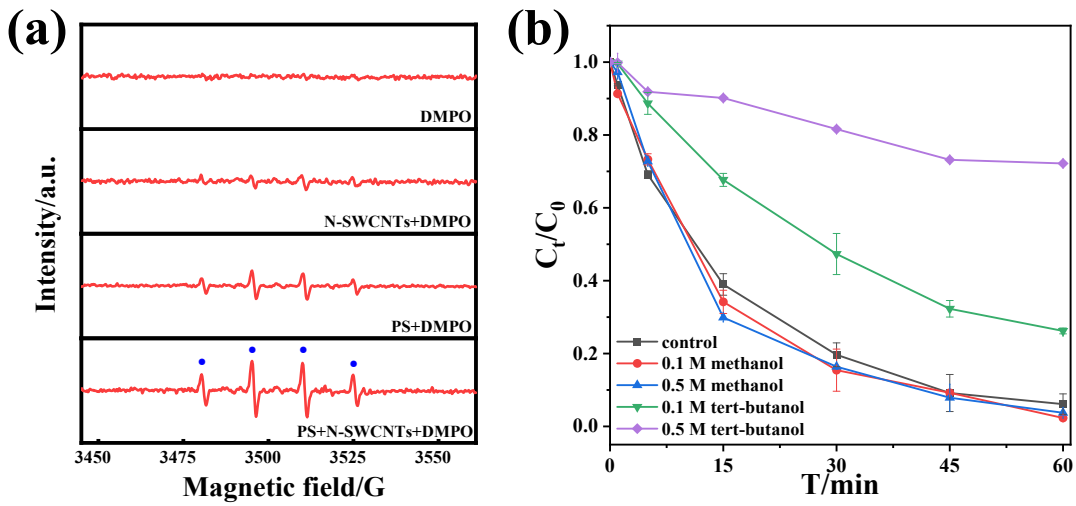


**Fig. S9.** EPR spectra in different systems obtained by spin trapping with 50 mM DMPO (a) and radical quenching experiments in PS/N-SWCNTs system (b). Conditions: $[BPS]_0$ = 10 μM, $[PS]_0$ = 1.0 mM, T = 25 ℃, $pH_0$ = 7.0, concentration of N-SWCNTs = 20 mg·$L^{-1}$.

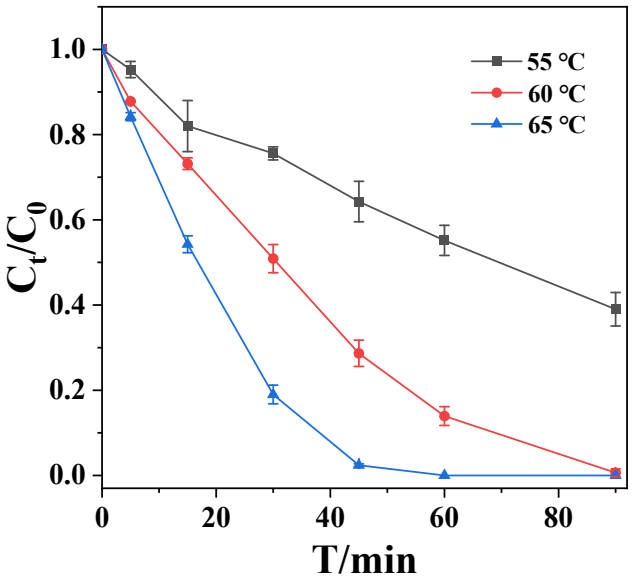


**Fig. S10.** Effect of temperature on the degradation of BPS in single PS system. Conditions: $[BPS]_0$ = 10 μM, $[PS]_0$ = 1.0 mM, $pH_0$ = 7.0.

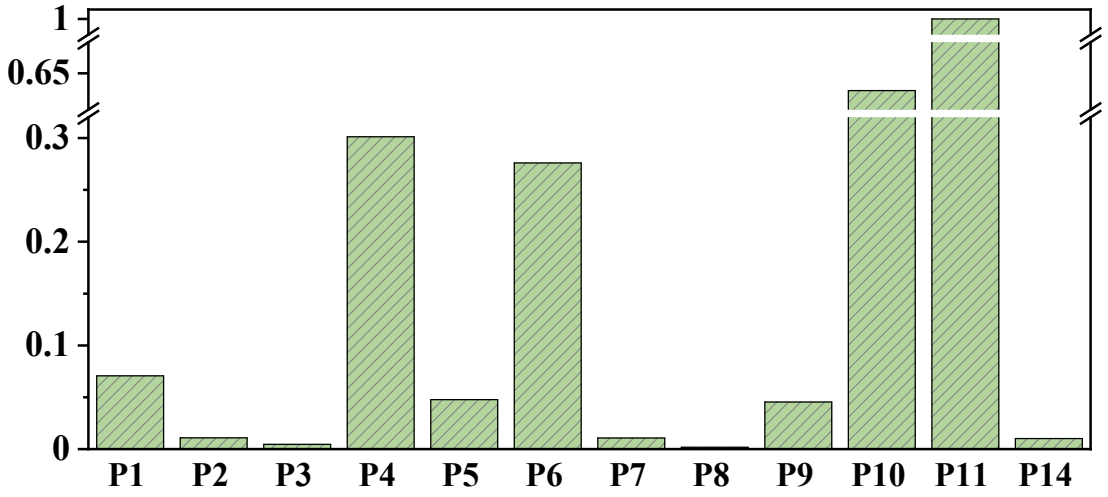


**Fig. S11.** The highest peak area of the identified intermediates in the PS/N-SWCNTs system. Note that the highest peak area (P11) is taken as 1 to calculate the relative yield of these 14 intermediates of BPS.

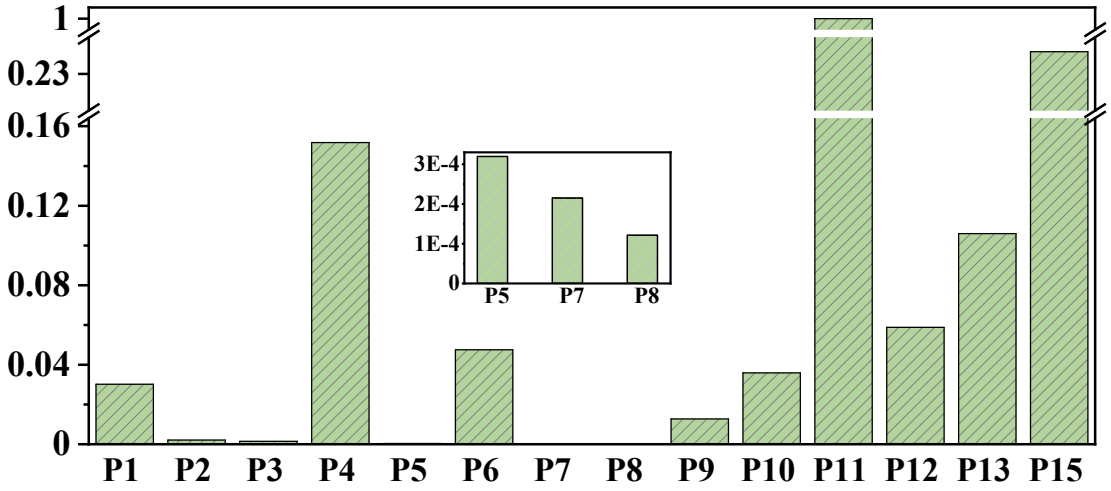


**Fig. S12.** The highest peak area of the identified intermediates in the PS-heat system. Note that the highest peak area (P11) is taken as 1 to calculate the relative yield of these 15 intermediates of BPS.

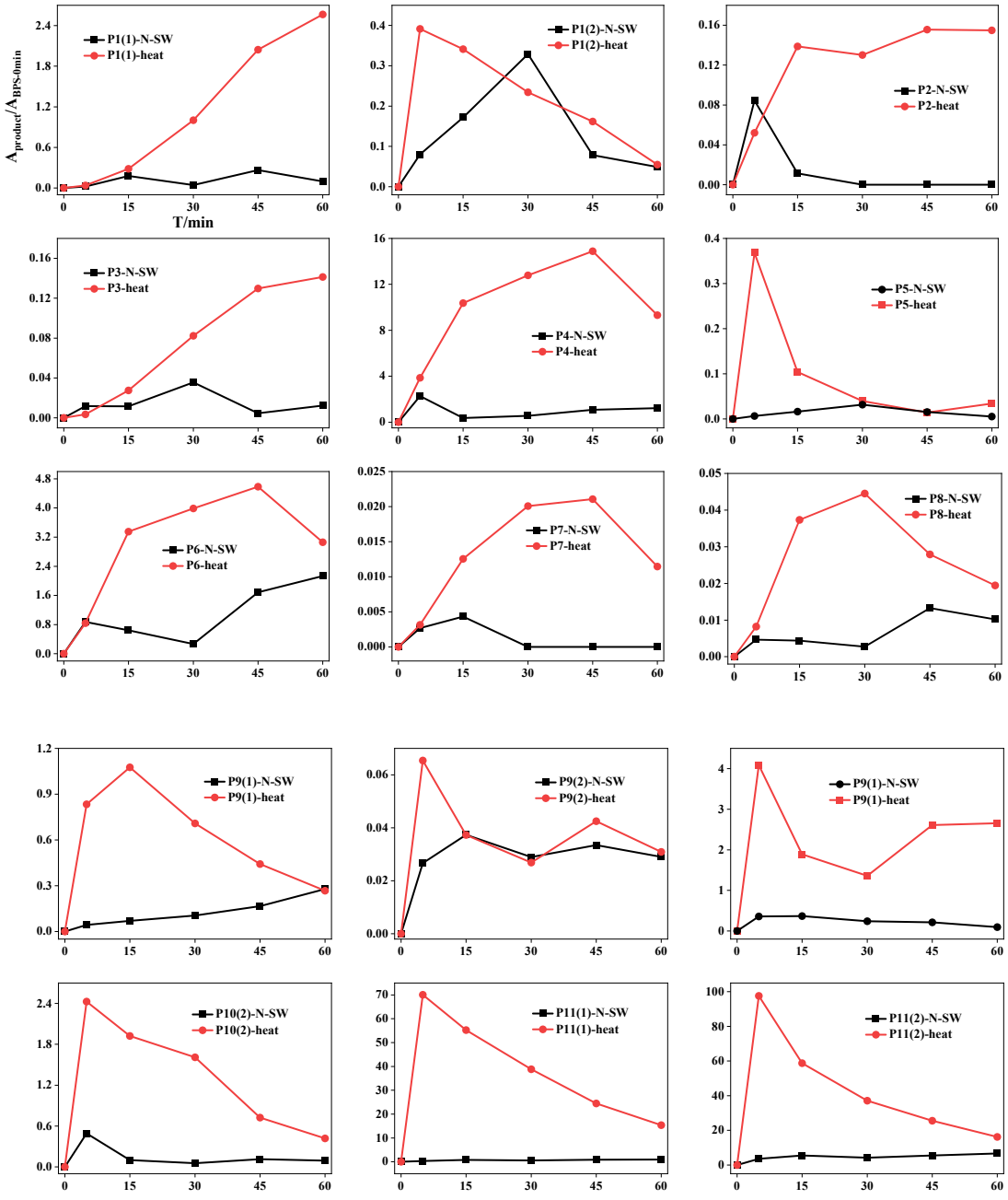


**Fig. S13.** Changes in the relative contents of common BPS transformation products in two systems. ($A_{product}$: the peak area of each product at each sampling time; $A_{BPS\text{-}0min}$: the peak area of BPS at 0 min)

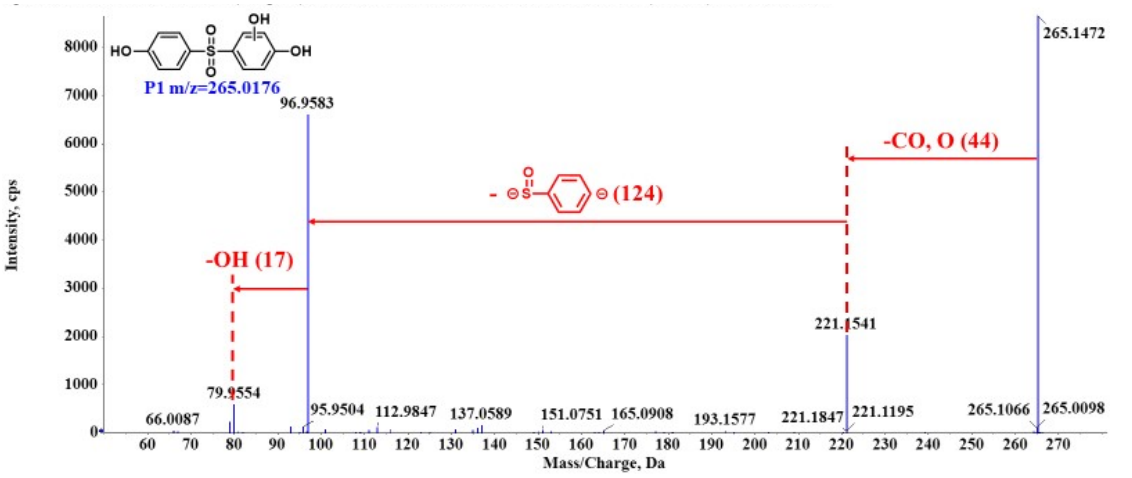
P1 m/z=265.0176
Intensity, cps
Mass/Charge, Da
265.1472
96.9583
-CO, O (44)
- (124)
-OH (17)
221.1541
79.9554
66.0087
95.9504
112.9847
137.0589
151.0751
165.0908
193.1577
221.1847
221.1195
265.1066
265.0098

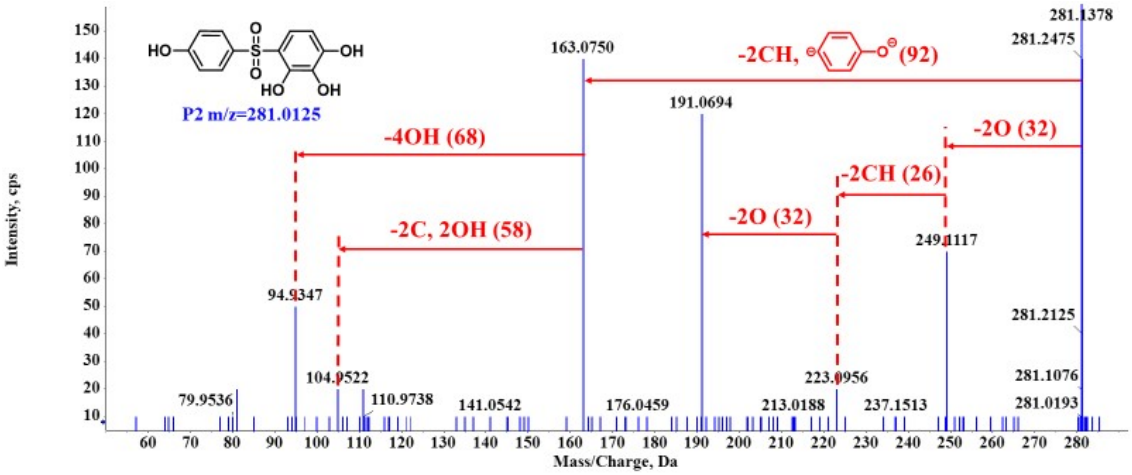
P2 m/z=281.0125
Intensity, cps
Mass/Charge, Da
281.1378
281.2475
163.0750
-2CH, (92)
191.0694
-4OH (68)
-2O (32)
-2CH (26)
-2C, 2OH (58)
-2O (32)
249.1117
94.9347
281.2125
104.9522
223.0956
281.1076
79.9536
110.9738
141.0542
176.0459
213.0188
237.1513
281.0193

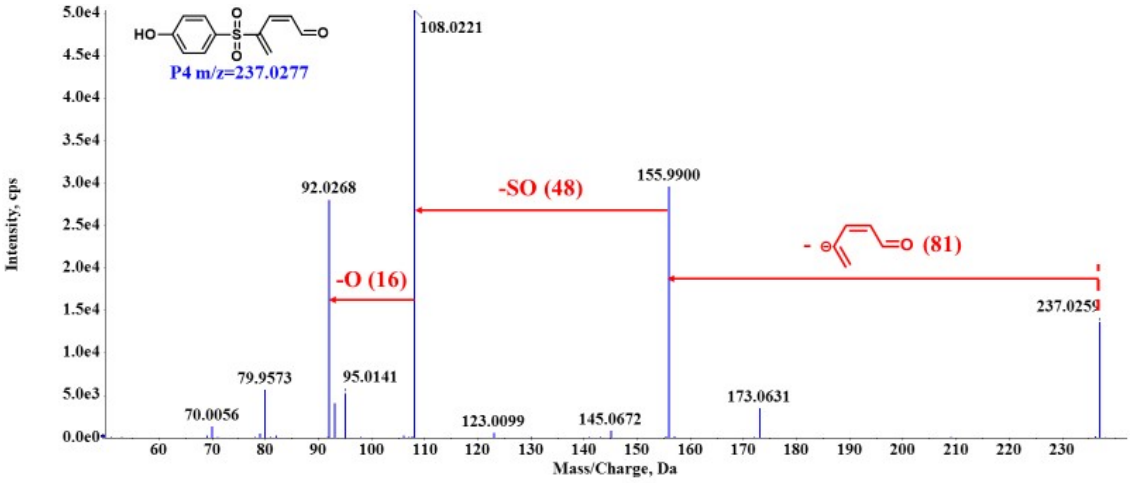
P4 m/z=237.0277
Intensity, cps
Mass/Charge, Da
108.0221
92.0268
-SO (48)
155.9900
- (81)
-O (16)
237.0259
79.9573
95.0141
70.0056
123.0099
145.0672
173.0631

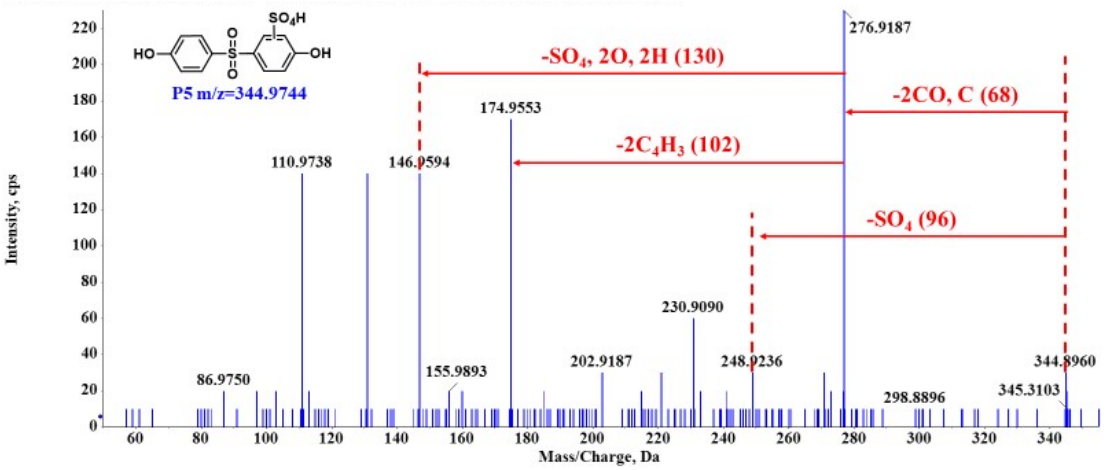
P5 m/z=344.9744
-SO4, 2O, 2H (130)
-2CO, C (68)
-2C4H3 (102)
-SO4 (96)
276.9187
174.9553
110.9738
146.9594
230.9090
155.9893
202.9187
248.9236
344.8960
86.9750
298.8896
345.3103
Intensity, cps
Mass/Charge, Da

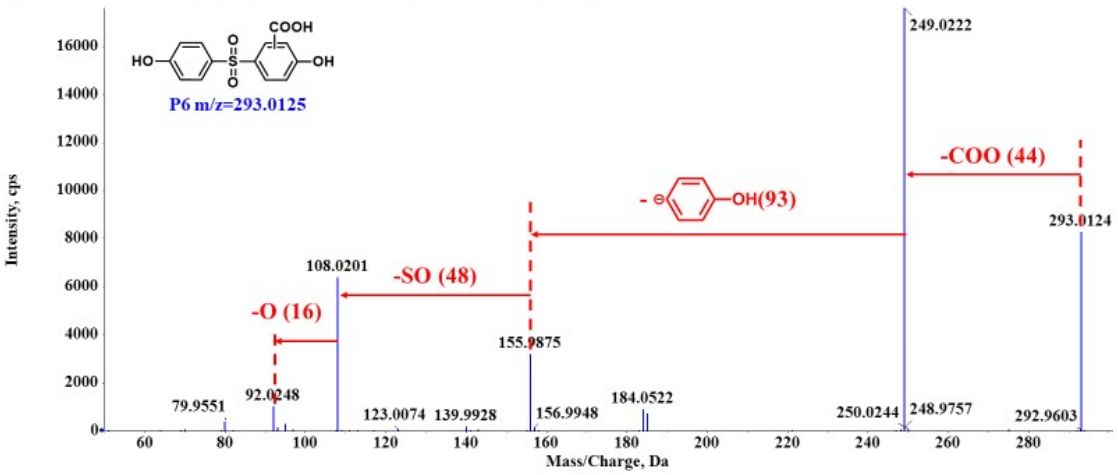
P6 m/z=293.0125
249.0222
-COO (44)
-OH(93)
293.0124
108.0201
-SO (48)
-O (16)
155.9875
92.0248
79.9551
123.0074
139.9928
156.9948
184.0522
250.0244
248.9757
292.9603
Intensity, cps
Mass/Charge, Da

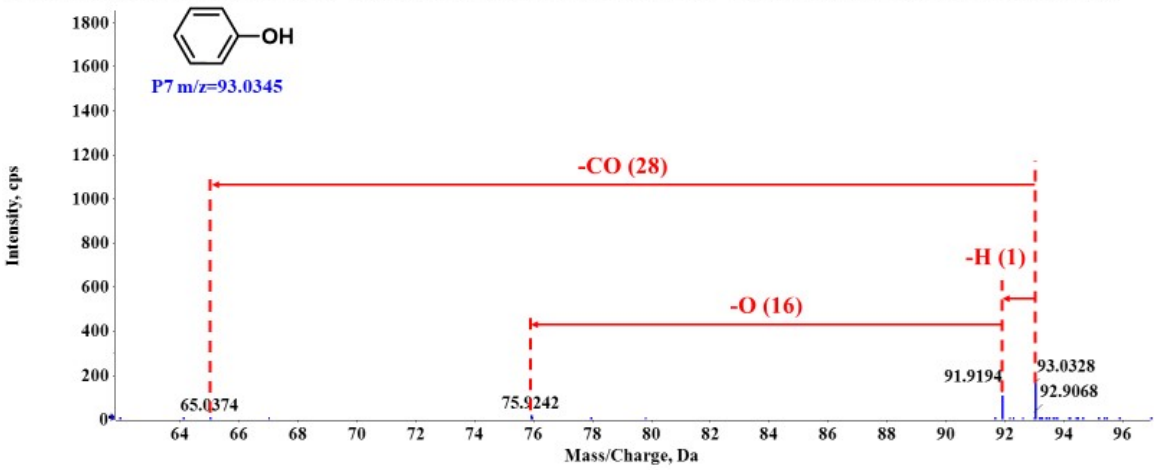
P7 m/z=93.0345
-CO (28)
-H (1)
-O (16)
93.0328
91.9194
92.9068
65.0374
75.9242
Intensity, cps
Mass/Charge, Da

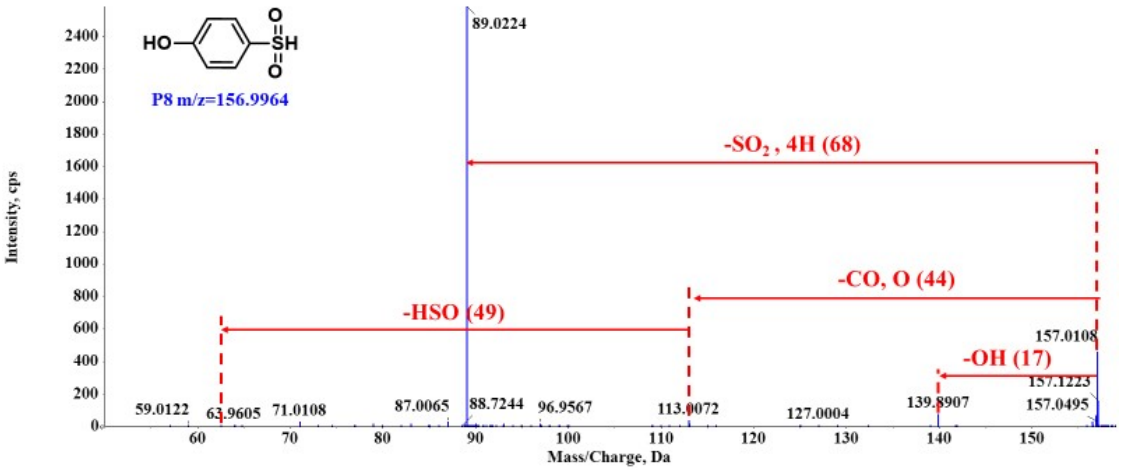
P8 m/z=156.9964
89.0224
-SO2 , 4H (68)
-CO, O (44)
-HSO (49)
157.0108
-OH (17)
157.1225
157.0495
59.0122
63.9605
71.0108
87.0065
88.7244
96.9567
113.0072
127.0004
139.8907
Intensity, cps
Mass/Charge, Da

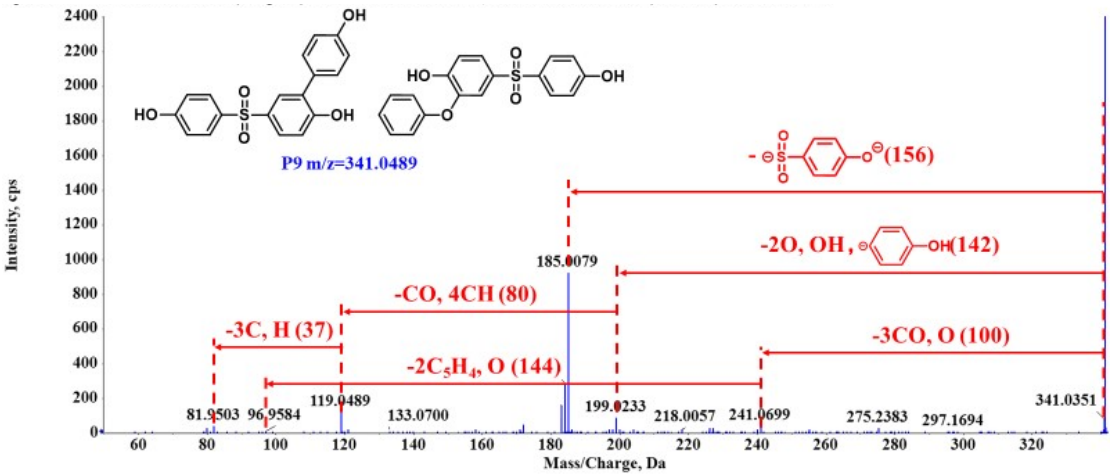
P9 m/z=341.0489
(156)
-2O, OH, (142)
185.0079
-CO, 4CH (80)
-3C, H (37)
-3CO, O (100)
-2C5H4, O (144)
81.9503
96.9584
119.0489
133.0700
199.0233
218.0057
241.0699
275.2383
297.1694
341.0351
Intensity, cps
Mass/Charge, Da

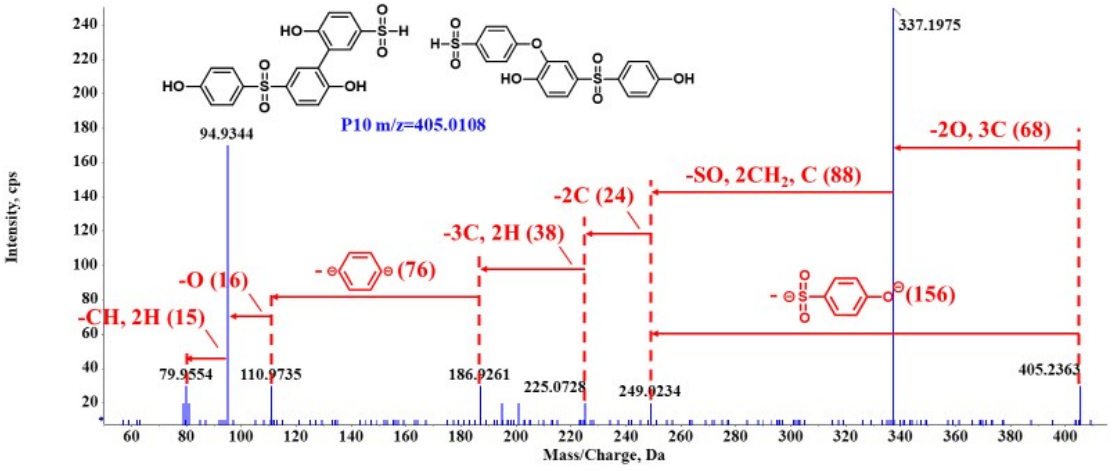
P10 m/z=405.0108
337.1975
94.9344
-2O, 3C (68)
-SO, 2CH2, C (88)
-2C (24)
-3C, 2H (38)
(76)
-O (16)
(156)
-CH, 2H (15)
79.9554
110.9735
186.9261
225.0728
249.9234
405.2363
Intensity, cps
Mass/Charge, Da

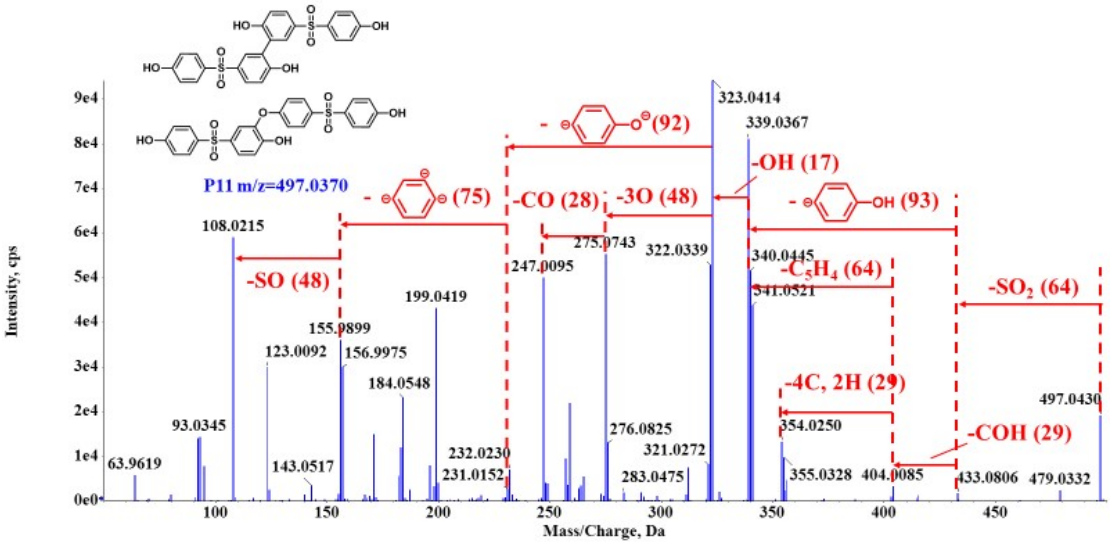
P11 m/z=497.0370
Intensity, cps
Mass/Charge, Da
323.0414
339.0367
-(92)
-OH (17)
-(75)
-CO (28)
-3O (48)
-OH (93)
-SO (48)
-C5H4 (64)
-SO2 (64)
-4C, 2H (29)
-COH (29)
108.0215
247.0095
275.0743
322.0339
340.0445
541.0521
199.0419
155.9899
123.0092
156.9975
184.0548
497.0430
354.0250
93.0345
276.0825
321.0272
63.9619
143.0517
232.0230
231.0152
283.0475
355.0328
404.0085
433.0806
479.0332

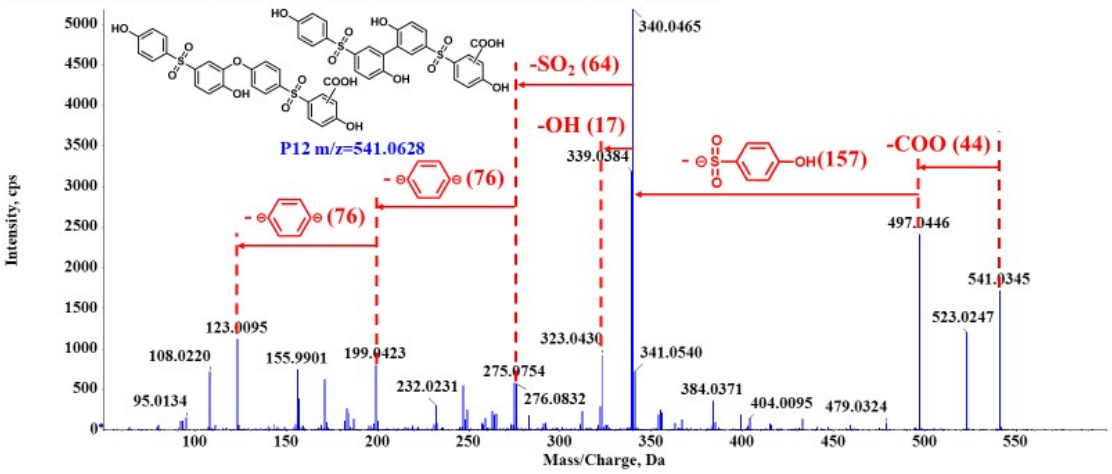
P12 m/z=541.0628
Intensity, cps
Mass/Charge, Da
340.0465
-SO2 (64)
-OH (17)
339.0384
-(157)
-COO (44)
-(76)
-(76)
497.0446
541.0345
523.0247
123.0095
108.0220
155.9901
199.9423
323.0430
341.0540
275.0754
232.0231
276.0832
384.0371
404.0095
479.0324
95.0134

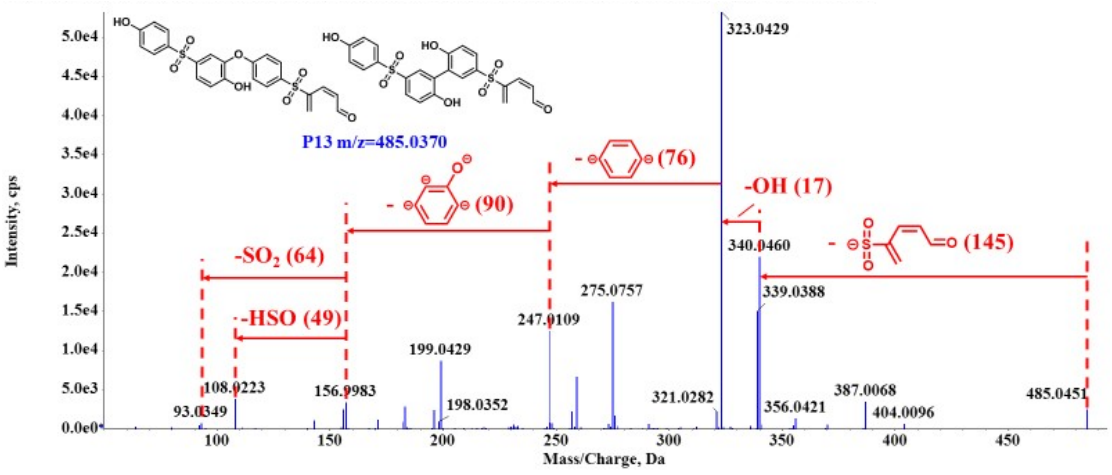
P13 m/z=485.0370
Intensity, cps
Mass/Charge, Da
323.0429
-(76)
-(90)
-OH (17)
340.0460
-(145)
-SO2 (64)
-HSO (49)
275.0757
339.0388
247.0109
199.0429
108.0223
156.9983
198.0352
321.0282
387.0068
485.0451
93.0349
356.0421
404.0096

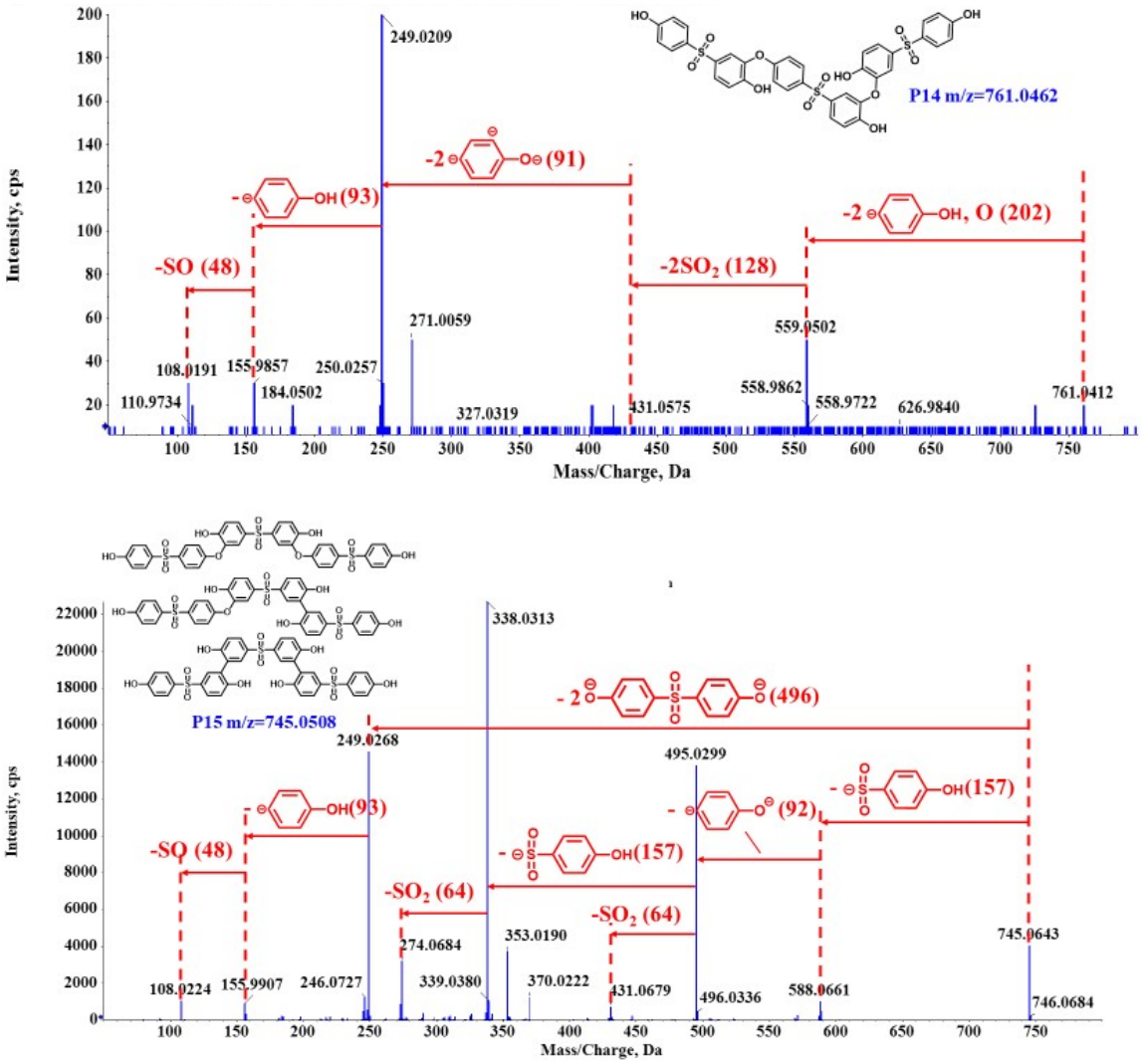


**Fig. S14.** The MS/MS spectra of 15 products in our two studied systems.

**Table. S1.** Technical data for nanocarbon-based materials.

| Property | Purity | Outer Diameter | Length | Thickness |
|---|---|---|---|---|
| MWCNTs | >95 | 20-30 nm | 10-30 μm | |
| SWCNTs | 90 | <2 nm | 5-15 μm | |
| CNT-OH | >95 | 20-30 nm | 10-30 μm | |
| GP | >98 | | | 6-8 nm |
| GO | >95 | 0.5-5 μm | | 1-3 nm |

**Table. S2.** Elemental composition of (N-)SWCNTs.

| Samples | Atom Composition | | |
|---|---|---|---|
| | C1s | N1s | O1s |
| SWCNTs | 97.89 | - | 2.11 |
| N-SWCNTs | 96.25 | 1.16 | 2.58 |

**Table. S3.** Specific surface area of nanocarbon-based materials.

| Samples | BET specific surface area ($m^2 \cdot g^{-1}$) | |
|---|---|---|
| | commercial | N doping |
| MWCNTs | 208.09 | 314.09 |
| SWCNTs | 560.44 | 619.59 |
| CNT-OH | 195.20 | 275.24 |
| GO | 0.31 | 127.16 |
| GP | 85.01 | 79.73 |

**Table. S4.** Water quality parameters of four water samples.*

| Parameter | Unit | Tap water | River water | Secondary effluent |
|---|---|---|---|---|
| pH | -- | 6.95 | 7.47 | 7.27 |
| TOC | $mg \cdot L^{-1}$ | 3.15 | 19.98 | 22.08 |
| $Cl^-$ | $mg \cdot L^{-1}$ | 14.27 | 42.15 | 269.63 |
| $NO_3^-$ | $mg \cdot L^{-1}$ | 9.61 | 58.93 | 52.76 |
| $HCO_3^-$ | $mg \cdot L^{-1}$ | ND | ND | ND |
| $SO_4^{2-}$ | $mg \cdot L^{-1}$ | 38.58 | 144.19 | 139.28 |
| Na | $mg \cdot L^{-1}$ | 4.79 | 8.12 | 60.41 |
| Mg | $mg \cdot L^{-1}$ | 5.14 | 7.60 | 17.44 |
| K | $mg \cdot L^{-1}$ | 2.44 | 4.67 | 11.52 |
| Ca | $mg \cdot L^{-1}$ | 3.04 | 6.29 | 4.91 |

* Total organic carbon (TOC) was measured by a TOC analyzer (Elementar, Germany). The concentrations of anions and metal ions were detected by ICS-5000 (Dionex, USA) and ICP-MS (NexION 300x, USA), respectively. ND: Not detected.

**Table. S5.** Mass measurements for the intermediates of BPS by LC-TOF-MS/MS analysis.

| Compound | $R_t$/min | Molecular formula | Measured mass | Theoretical mass | Error/ppm |
|---|---|---|---|---|---|
| P1 | 5.962 | $C_{12}H_{10}O_5S$ | 265.0180 | 265.0176 | -1.51 |
| | 7.018 | $C_{12}H_{10}O_5S$ | 265.0184 | 265.0176 | -3.02 |
| P2 | 7.035 | $C_{12}H_{10}O_6S$ | 281.0127 | 281.0125 | -0.71 |
| P3 | 5.972 | $C_{12}H_8O_5S$ | 263.0017 | 263.0014 | -1.14 |
| P4 | 5.671 | $C_{11}H_{10}O_4S$ | 237.0229 | 237.0227 | -0.84 |
| P5 | 6.038 | $C_{12}H_{10}O_8S_2$ | 344.9754 | 344.9744 | -2.90 |
| P6 | 7.752 | $C_{13}H_{10}O_6S$ | 293.0128 | 293.0125 | -1.02 |
| P7 | 8.124 | $C_6H_6O$ | 93.0339 | 93.0345 | 6.45 |
| P8 | 1.669 | $C_6H_6O_3S$ | 156.9965 | 156.9964 | -0.64 |
| P9 | 9.148 | $C_{18}H_{14}O_5S$ | 341.0494 | 341.0489 | -1.47 |
| | 9.86 | $C_{18}H_{14}O_5S$ | 341.0495 | 341.0489 | -1.76 |
| P10 | 7.932 | $C_{18}H_{14}O_7S_2$ | 405.0117 | 405.0108 | -2.22 |
| | 9.849 | $C_{18}H_{14}O_7S_2$ | 405.0116 | 405.0108 | -1.98 |
| P11 | 8.367 | $C_{24}H_{18}O_8S_2$ | 497.0376 | 497.0370 | -1.21 |
| | 9.657 | $C_{24}H_{18}O_8S_2$ | 497.0375 | 497.0370 | -1.01 |
| P12 | 10.204 | $C_{25}H_{18}O_{10}S_2$ | 541.0249 | 541.0268 | 3.51 |
| | 10.807 | $C_{25}H_{18}O_{10}S_2$ | 541.0248 | 541.0268 | 3.70 |
| P13 | 8.622 | $C_{23}H_{18}O_8S_2$ | 485.0355 | 485.0370 | 3.09 |
| | 10.215 | $C_{23}H_{18}O_8S_2$ | 485.0359 | 485.0370 | 2.27 |
| P14 | 9.443 | $C_{36}H_{26}O_{13}S_3$ | 761.0463 | 761.0462 | -0.13 |
| P15 | 10.342 | $C_{36}H_{26}O_{12}S_3$ | 745.0473 | 745.0508 | 4.70 |
| | 10.555 | $C_{36}H_{26}O_{12}S_3$ | 745.0479 | 745.0508 | 3.89 |
| | 10.746 | $C_{36}H_{26}O_{12}S_3$ | 745.0475 | 745.0508 | 4.43 |

**Table. S6.** The atom coordinates for calculation of $SO_4^{\bullet-}$ initiated RAF reaction in Gaussian 09 program.

| atom | x | y | z |
|---|---|---|---|
| C | -2.77674 | -1.62518 | -1.00861 |
| C | -2.52249 | -0.88994 | 0.18571 |
| C | -1.25268 | -1.04226 | 0.81059 |
| C | -0.27278 | -1.76418 | 0.14162 |
| C | -0.49424 | -2.42131 | -1.0739 |
| C | -1.77203 | -2.36006 | -1.6456 |
| O | -4.06344 | -1.55252 | -1.49375 |
| H | -4.14757 | -1.85083 | -2.41874 |
| H | -3.35312 | -0.45956 | 0.73706 |
| H | -1.05853 | -0.56731 | 1.76848 |
| H | 0.30955 | -2.98911 | -1.53256 |
| H | -1.98061 | -2.88522 | -2.57372 |
| S | 1.40272 | -1.88473 | 0.87798 |
| O | 2.14338 | -3.17389 | 0.20358 |
| O | 1.23941 | -1.80372 | 2.49371 |
| C | 2.28677 | -0.40585 | 0.2422 |
| C | 3.50946 | -0.60279 | -0.40526 |
| C | 4.18252 | 0.51972 | -0.89646 |
| C | 3.61025 | 1.79169 | -0.73608 |
| C | 2.37763 | 1.96213 | -0.08867 |
| C | 1.70303 | 0.84674 | 0.41964 |
| O | 4.3222 | 2.8686 | -1.26002 |
| H | 3.90178 | -1.60763 | -0.5247 |
| H | 5.13392 | 0.43634 | -1.40827 |
| H | 3.84895 | 3.71416 | -1.14492 |
| H | 1.91256 | 2.93903 | 0.01699 |
| H | 0.7323 | 1.00897 | 0.89016 |
| S | -2.26531 | 2.11118 | 0.42343 |
| O | -0.76867 | 2.13546 | 1.04459 |
| O | -3.37494 | 1.62765 | 1.49865 |
| O | -2.64047 | 3.39652 | -0.47432 |
| O | -2.22869 | 0.8251 | -0.80035 |

Note: Take C (2) as an example.

**Table. S7.** The atom coordinates for calculation of •OH initialed RAF reaction in Gaussian 09 program.

| atom | x | y | z |
|---|---|---|---|
| C | -3.565759 | -0.628119 | -0.47051 |
| C | -3.045488 | -0.599251 | 0.862995 |
| C | -1.859833 | 0.148841 | 1.105092 |
| C | -1.24508 | 0.772189 | 0.030827 |
| C | -1.779931 | 0.788113 | -1.268329 |
| C | -2.95556 | 0.072889 | -1.517277 |
| O | -4.667769 | -1.395766 | -0.741453 |
| H | -4.711102 | -2.160599 | -0.12684 |
| H | -3.700013 | -0.838153 | 1.692587 |
| H | -1.46317 | 0.257308 | 2.109696 |
| H | -1.285464 | 1.361576 | -2.046796 |
| H | -3.398935 | 0.025627 | -2.504105 |
| S | 0.303449 | 1.714396 | 0.338942 |
| O | 0.295406 | 2.111015 | 1.916550 |
| O | 0.425480 | 2.808456 | -0.859201 |
| C | 1.667926 | 0.512416 | 0.096774 |
| C | 2.083081 | -0.250308 | 1.192205 |
| C | 3.126792 | -1.159074 | 1.010912 |
| C | 3.733495 | -1.272147 | -0.251054 |
| C | 3.318309 | -0.477454 | -1.332756 |
| C | 2.270111 | 0.434170 | -1.157164 |
| O | 4.759678 | -2.195192 | -0.356575 |
| H | 1.619384 | -0.108145 | 2.163740 |
| H | 3.495734 | -1.775153 | 1.821670 |
| H | 5.175838 | -2.225599 | -1.238475 |
| H | 3.811979 | -0.561097 | -2.296942 |
| H | 1.944814 | 1.088206 | -1.960327 |
| O | -2.689937 | -2.567400 | 0.881895 |
| H | -1.815492 | -2.636802 | 0.422707 |

Note: Take C (2) as an example.

**Table. S8.** The atom coordinates for calculation of •OH initialed HAA reaction in Gaussian 09 program.

| atom | x | y | z |
|---|---|---|---|
| C | -3.34474 | -0.64609 | -0.55203 |
| C | -2.82614 | -0.62688 | 0.75917 |
| C | -1.64136 | 0.06778 | 1.01642 |
| C | -0.99905 | 0.70193 | -0.049 |
| C | -1.50546 | 0.71659 | -1.35019 |
| C | -2.70069 | 0.03856 | -1.6006 |
| O | -4.47767 | -1.3496 | -0.87865 |
| H | -5.06926 | -1.67777 | -0.08032 |
| H | -3.36712 | -1.12255 | 1.5585 |
| H | -1.23647 | 0.14542 | 2.02082 |
| H | -0.99159 | 1.2742 | -2.12725 |
| H | -3.15112 | 0.01827 | -2.58567 |
| S | 0.55477 | 1.62107 | 0.29133 |
| O | 0.50318 | 2.05896 | 1.85799 |
| O | 0.74027 | 2.68674 | -0.92472 |
| C | 1.91288 | 0.39792 | 0.13145 |
| C | 2.29447 | -0.32616 | 1.26424 |
| C | 3.33637 | -1.24724 | 1.14305 |
| C | 3.97359 | -1.41123 | -0.09768 |
| C | 3.59155 | -0.6551 | -1.21847 |
| C | 2.54576 | 0.26845 | -1.10292 |
| O | 4.9963 | -2.3443 | -0.14318 |
| H | 1.80629 | -0.14523 | 2.21697 |
| H | 3.67898 | -1.83626 | 1.98496 |
| H | 5.42629 | -2.41567 | -1.01608 |
| H | 4.10773 | -0.77799 | -2.16648 |
| H | 2.24444 | 0.89345 | -1.93792 |
| O | -5.93658 | -1.43305 | 0.92486 |
| H | -6.75163 | -0.91421 | 0.72025 |

Note: Take H (1) as an example.

## References


1. X. Pan, L. Yan, R. Qu and Z. Wang, Degradation of the UV-filter benzophenone-3 in aqueous solution using persulfate activated by heat, metal ions and light, *Chemosphere*, 2018, **196**, 95-104.
2. H. Liu, P. Sun, M. Feng, H. Liu, S. Yang, L. Wang and Z. Wang, Nitrogen and sulfur co-doped CNT-COOH as an efficient metal-free catalyst for the degradation of UV filter BP-4 based on sulfate radicals, *Appl. Catal., B*, 2016, **187**, 1-10.
3. A. Nasiri, M. Shariaty-Niasar, A. M. Rashidi and R. Khodafarin, Effect of CNT structures on thermal conductivity and stability of nanofluid, *Int. J. Heat Mass Transfer*, 2012, **55**, 1529-1535.
4. J. Kang, X. Duan, C. Wang, H. Sun, X. Tan, M. O. Tade and S. Wang, Nitrogen-doped bamboo-like carbon nanotubes with Ni encapsulation for persulfate activation to remove emerging contaminants with excellent catalytic stability, *Chem. Eng. J.*, 2018, **332**, 398-408.
5. Y. Pang, K. Luo, L. Tang, X. Li, Y. Song, C.-y. Li and L.-p. Wang, Preparation and application of magnetic nitrogen-doped rGO for persulfate activation, *Environmental Science and Pollution Research*, 2018, **25**, 30575-30584.
6. J. Yu, L. Tang, Y. Pang, G. Zeng, J. Wang, Y. Deng, Y. Liu, H. Feng, S. Chen and X. Ren, Magnetic nitrogen-doped sludge-derived biochar catalysts for persulfate activation: Internal electron transfer mechanism, *Chem. Eng. J.*, 2019, **364**, 146-159.
7. X.-K. Kong, C.-L. Chen and Q.-W. Chen, Doped graphene for metal-free catalysis, *Chem. Soc. Rev.*, 2014, **43**, 2841-2857.
8. J. Zhang, D. S. Su, R. Blume, R. Schlögl, R. Wang, X. Yang and A. Gajović, Surface chemistry and catalytic reactivity of a nanodiamond in the steam‐free dehydrogenation of ethylbenzene, *Angew. Chem.*, 2010, **122**, 8822-8826.
9. X. Duan, H. Sun, J. Kang, Y. Wang, S. Indrawirawan and S. Wang, Insights into Heterogeneous Catalysis of Persulfate Activation on Dimensional-Structured Nanocarbons, *ACS Catalysis*, 2015, **5**, 4629-4636.
10. X. Wang, Y. Qin, L. Zhu and H. Tang, Nitrogen-doped reduced graphene oxide as a bifunctional material for removing bisphenols: synergistic effect between adsorption and catalysis, *Environ. Sci. Technol.*, 2015, **49**, 6855-6864.
11. X. Duan, Z. Ao, H. Sun, L. Zhou, G. Wang and S. Wang, Insights into N-doping in single-walled carbon nanotubes for enhanced activation of superoxides: a mechanistic study, *Chem. Commun. (Cambridge, U. K.)*, 2015, **51**, 15249-15252.
12. X. Cheng, H. Guo, Y. Zhang, X. Wu and Y. Liu, Non-photochemical production of singlet oxygen via activation of persulfate by carbon nanotubes, *Water Res.*, 2017, **113**, 80-88.
13. P. Shao, J. Tian, F. Yang, X. Duan, S. Gao, W. Shi, X. Luo, F. Cui, S. Luo and S. Wang, Identification and regulation of active sites on nanodiamonds: establishing a highly efficient catalytic system for oxidation of organic contaminants, *Adv. Funct. Mater.*, 2018, **28**, 1705295.
14. X. Cheng, H. Guo, Y. Zhang, G. V. Korshin and B. Yang, Insights into the mechanism of nonradical reactions of persulfate activated by carbon nanotubes: Activation performance and structure-function relationship, *Water Res.*, 2019, **157**, 406-414.
15. W. Ren, G. Nie, P. Zhou, H. Zhang, X. Duan and S. Wang, The Intrinsic Nature of Persulfate Activation and N-Doping in Carbocatalysis, *Environ. Sci. Technol.*, 2020, **54**, 6438-6447.
16. G. S. Timmins, K. J. Liu, E. J. H. Bechara, Y. Kotake and H. M. Swartz, Trapping of free radicals with direct in vivo EPR detection: a comparison of 5,5-dimethyl-1-pyrroline-N-oxide and 5-

diethoxyphosphoryl-5-methyl-1-pyrroline-N-oxide as spin traps for HO and SO4•−, *Free Radic. Biol. Med.*, 1999, **27**, 329-333.

17. H. Lee, H.-J. Lee, J. Jeong, J. Lee, N.-B. Park and C. Lee, Activation of persulfates by carbon nanotubes: Oxidation of organic compounds by nonradical mechanism, *Chem. Eng. J.*, 2015, **266**, 28-33.